

Iran atlas of offshore renewable energies

M. Abbaspour, R. Rahimi*

Sharif University of Technology, School of Mechanical engineering, Azadi Ave., Tehran, Iran

ARTICLE INFO

Article history:

Received 30 January 2010

Accepted 30 June 2010

Available online 6 August 2010

Keywords:

Offshore Renewable Energy

Atlas

Tide

Wave

Iran

ABSTRACT

The aim of the present study is to provide an Atlas of IRAN Offshore Renewable Energy Resources (hereafter called 'the Atlas') to map out wave and tidal resources at a national scale, extending over the area of the Persian Gulf and Sea of Oman. Such an Atlas can provide necessary tools to identify the areas with greatest resource potential and within reach of present technology development.

To estimate available tidal energy resources at the site, a two-dimensional tidally driven hydrodynamic numerical model of Persian Gulf was developed using the hydrodynamic model in the MIKE 21 Flow Model (MIKE 21HD), with validation using tidal elevation measurements and tidal stream diamonds from Admiralty charts. The results of the model were used to produce a time series of the tidal stream velocity over the simulation period.

Moreover, to assess the potential of the wave energy in this site, a model was developed based on six-hourly data from a third generation ocean wave model (ISWM-Iranian Sea Wave Model) covering the period 1992–2003.

To ensure the information provided to the Atlas is managed and maintained most effectively, all the derived marine resource parameters have been captured in a structured database, within a Geographical Information System (GIS), so enabling effective data management, presentation and interrogation.

© 2010 Elsevier Ltd. All rights reserved.

1. Introduction

There is a growing expectation that the energy resources created by the dynamics of the marine environment will be able to make a real and measurable contribution to the Renewables Agenda over the next 10 years and beyond, both nationally and globally. However, what has presently been unavailable is any detailed quantification of this resource (waves, tides and offshore winds).

Before IRAN can adopt any large-scale deployment of energy converters in the marine environment the Government should conduct a comprehensive study of the issues relevant to such a program of development. Prior to any future rounds for wave, tidal or offshore wind it is therefore relevant that a study is undertaken to survey the potential marine energy resource over the scale of the Persian Gulf to inform the planning process and assist in future site selection. It is also the purpose of this study to consider the whole of the marine environment despite the fact that some areas may not attract much attention from the marine renewable industry.

The approach taken has been to review the range of work already undertaken, and provide a more detailed and consistent description of the marine resource by making use of the best available data and

technical expertise. In order to have detailed information of wave and tidal resources two Numerical models developed and validated against best in-situ measurements available.

1.1. Area of interest

The area of interest includes the marine waters extending across the entire Persian Gulf bounded by the 21 – 34° N latitudes and 48 – 57° W longitudes off the coast of IRAN. The datasets used for the wave and tide analysis are acquired from the National Cartographic Center of Iran-Department of Hydrography, Iranian Meteorological Office, Iran Ports and Maritime Organization (PMO) and Iran National Centre of Oceanography (INCO).

2. Theoretical background

2.1. Tide

The kinetic energy passing through a vertical cross-section perpendicular to the flow direction per unit time, or the instantaneous theoretical tidal power density (energy flux) available in a tidal stream is given by:

$$P_{\text{Cross-section}} = 0.5\rho AU^3 \quad (1)$$

Where:

* Corresponding author. Tel./fax: +98 21 88375041.

E-mail addresses: m-abbaspour@jamejam.net (M. Abbaspour), r.rahimi@mech.sharif.edu (R. Rahimi).

$P_{\text{cross-section}}$ = theoretical power density (Watts)
 ρ = density of seawater (typically around 1025 kg/m³)
 A = cross-sectional area (m²)
 U = instantaneous current speed (m/s)

Hence, the mean power density per unit area of cross-sectional flow (per meter depth) and averaged over a defined tidal period (e.g. neap, spring or annual event) can be expressed as:

$$P_{\text{Mean power density}} = 0.5\rho [U^3] \quad (2)$$

With:

[] = chosen averaging period for time series data

It is important to note that final extractable power will be highly dependent on the physical characteristics of the site and the performance of the individual energy converter intercepting the resource. The dependency of the power output on a predictable pattern of tidal forces makes this type of energy converter very attractive to the energy supply market [1].

2.2. Wave

The energy flux or power (P) transmitted by a regular wave per unit crest width can be written as

$$P = \frac{1}{8}\rho g H^2 C_g \quad [kW/m] \quad (3)$$

Where ρ is the fluid density ($\sim 1.025 \frac{kg}{m^3}$), H is the wave height, and C_g is the group velocity, defined as

$$C_g = \frac{1}{2} \left(1 + \frac{2kh}{\sinh(2kh)} \right) \frac{L}{T} \quad (4)$$

In which h is the local water depth, L is the wave length, T is the wave period, $k = 2\pi/L$ is the wave number and $C = L/T$ is the wave celerity. The wave length, depth and period are related through the dispersion equation:

$$L = T \sqrt{\frac{g}{k} \tanh(kh)} \quad (5)$$

In shallow water ($h < L/2$), the following explicit equation for L can be used without noticeable error:

$$L = \frac{gT^2}{2\pi} \left\{ \tanh \left[\left(\frac{4\pi^2 h}{gT^2} \right)^{3/4} \right] \right\}^{2/3} \quad (6)$$

In deep water ($h > L/2$), $C = L/T = 2C_g$ and $L = L_0 = gT^2/2\pi$, therefore

$$P_0 = \frac{1}{32\pi} \rho g^2 H^2 T \quad (7)$$

Real sea states are often described as a summation of a large number of regular waves having different frequencies, amplitudes and directions. The mix of amplitudes, frequencies and directions is often described by a variance spectral density function or 2D wave spectrum $S(f,\theta)$. In this case, the power transmitted per unit width can be written as

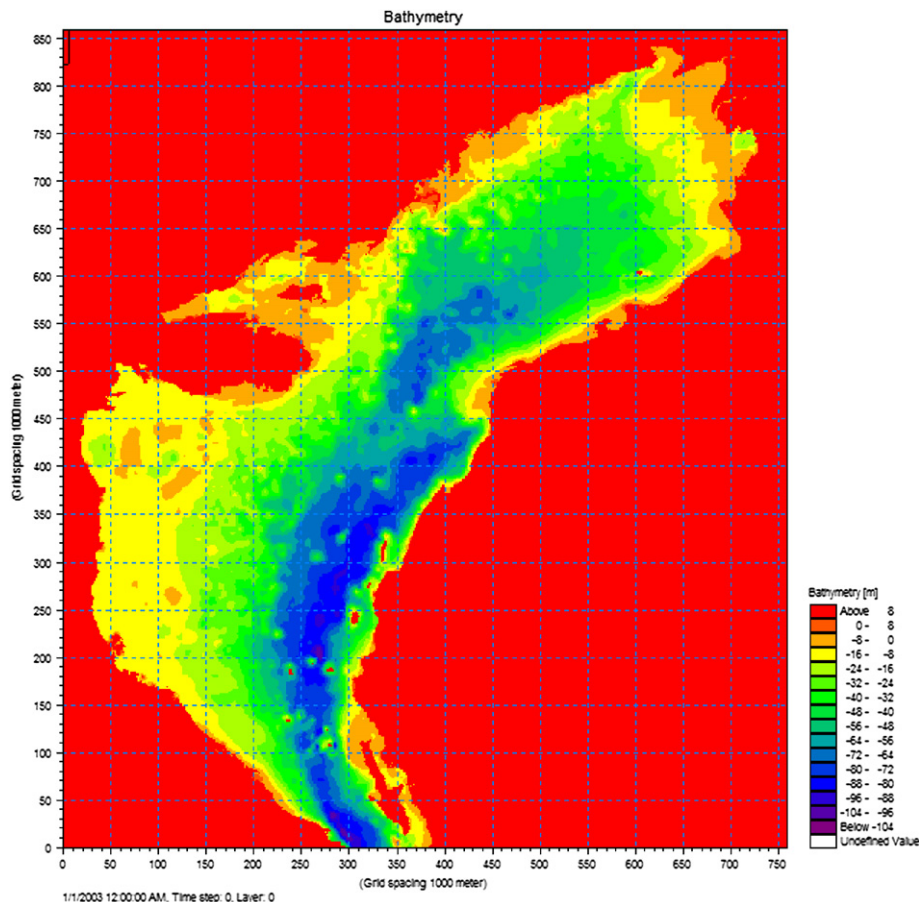


Fig. 1. Bathymetry – Grid Size 1000 m.

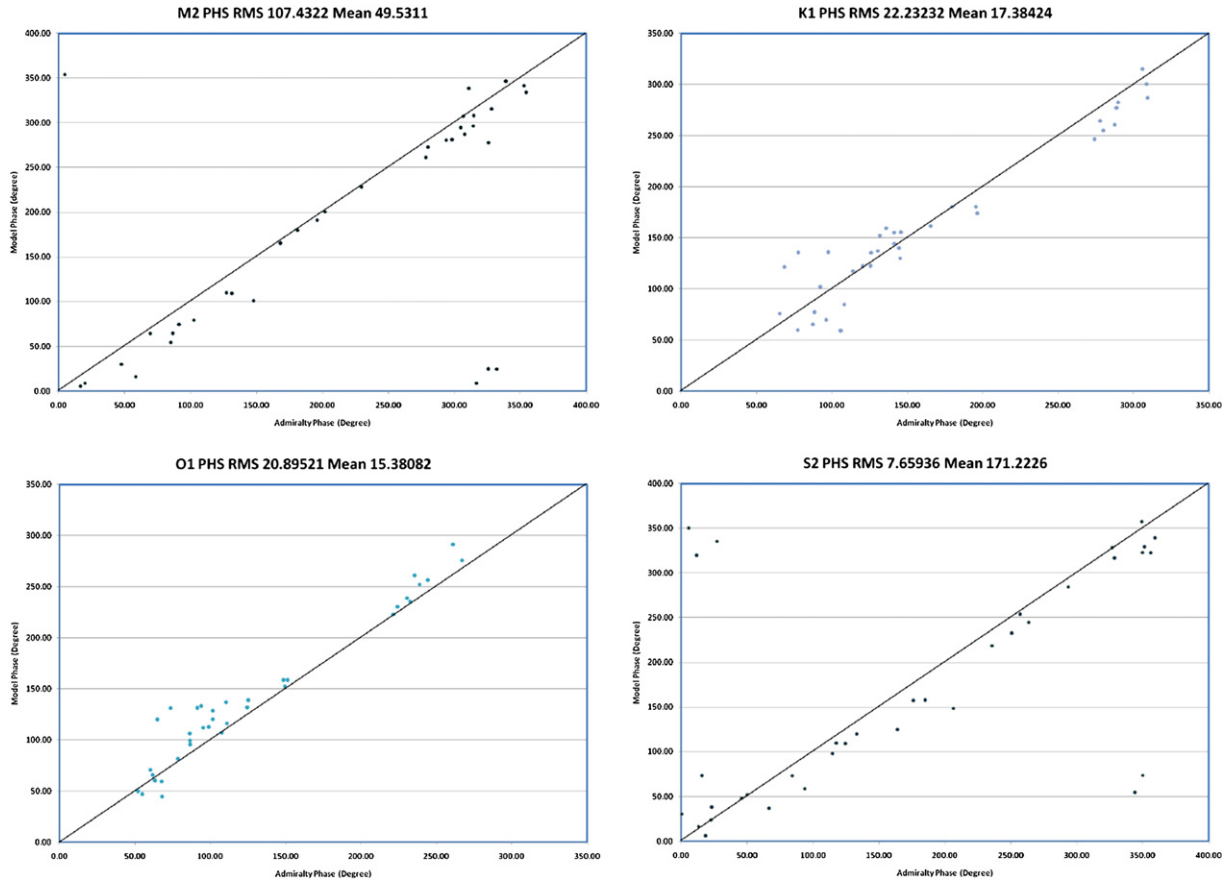


Fig. 2. Scatter Plots of model vs. observed tidal phases.

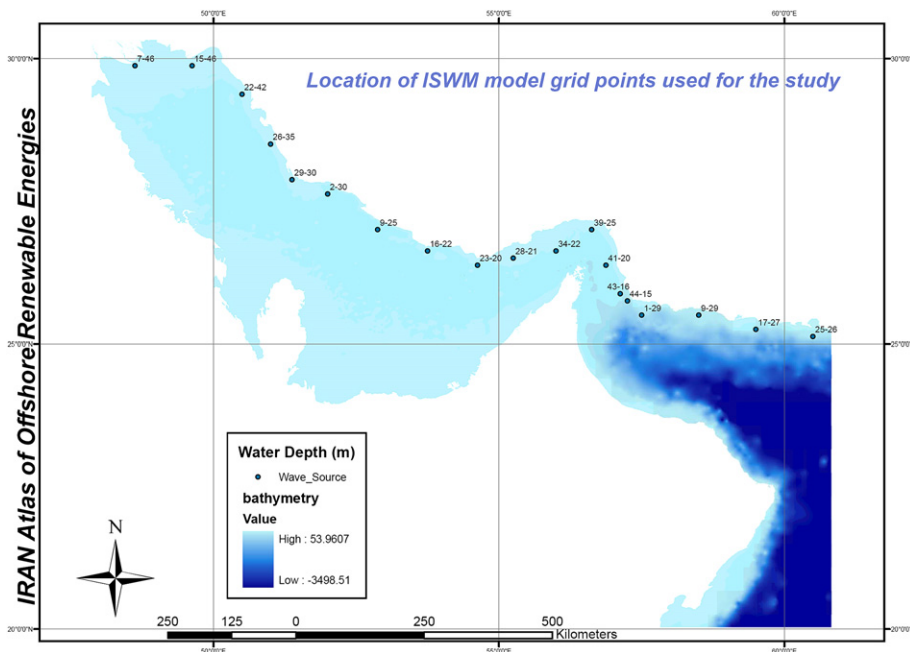


Fig. 3. Location of ISWM model grid used for the study.

Table 1
Error Statistics for Tidal Elevations.

Constituent	Phase (Degree)	
	RMS	Mean
O1	20.89521	15.38082
K1	22.23232	17.38424
M2	107.4322	49.5311
S2	7.65936	171.2226

$$P = \rho g \int_0^{2\pi} \int_0^\infty C_g(f, h) S(f, \theta) df d\theta \quad [kW/m] \quad (8)$$

With

$$C_g(f, h) = \frac{1}{2} \left[1 + \frac{2kh}{\sinh(2kh)} \right] \sqrt{\frac{g}{k} \tanh(kh)} \quad (9)$$

Where $k(f)$ is the frequency dependent wave number and h is the local water depth.

The wave power per unit width transmitted by the irregular waves can be approximated as

$$P \approx \frac{\rho g}{16} H_s^2 C_g(T_e, h) \quad [kW/m] \quad (10)$$

Where T_e is known as the energy period and $C_g(T_e, h)$ is the group velocity of a wave with period T_e in water depth h . The energy period of a sea state is defined in terms of spectral moments as

$$T_e = \frac{m_{-1}}{m_0} = \frac{\int_0^{2\pi} \int_0^\infty f^{-1} S(f) df d\theta}{\int_0^{2\pi} \int_0^\infty S(f) df d\theta} \quad (11)$$

In deep water ($h > L/2$), the approximate expression for wave power transmitted per unit width simplified further to

$$P_0 \approx \frac{\rho g^2}{64\pi} T_e H_s^2 \quad [kW/m] \quad (12)$$

Measured sea states are often specified in terms of significant wave height H_s and either peak period T_p or mean period T_z . The energy period T_e is rarely specified and must be estimated from other variables when the spectral shape is unknown. For example, in preparing the Atlas of UK Marine Renewable Energy Resources, it was assumed that $T_e = 1.14T_z$ [2]. Another approach when T_p is known is to assume

$$T_e = \alpha T_p \quad (13)$$

The coefficient α depends on the shape of the wave spectrum: $\alpha = 0.86$ for a Pierson–Moskowitz spectrum, and α increases towards unity with decreasing spectral width. In assessing the wave energy resource in southern New England, [3] assumed that $T_e = T_p$. In this study, we have adopted the more conservative assumption that $\alpha = 0.90$ or $T_e = 0.9T_p$, which is equivalent to assuming a standard JONSWAP spectrum with a peak enhancement factor of $\gamma = 0.33$ [4]. It is readily acknowledged that this necessary assumption introduces

Table 2
Coefficient values and format.

Parameter	Coefficient	Format
Wave Breaking	Gamma data = 1 and Alpha = 0.8	Constant
Bottom Friction	Nikuradse roughness	Varying in domain
White Capping	Dissipation Coefficient (Cdis, DELTA dis)	Varying in domain

Table 3
Buoy Stations used in validation study.

Time period	Parameters	Start date	End date	Station Name
A	Wave height, Period and Direction	15-March-1995 00:00	10-April-1995 21:00	Boushehr
B	Wave height, Period and Direction	05-May-1995 00:00	11-May-1995 21:00	Boushehr
C	Wave height, Period and Direction	15-November-1995 00:00	19-November-1995 21:00	Boushehr
D	Wave height, Period and Direction	31-November-2002 00:00	10-December-2002 21:00	Assalouieh

some uncertainty into the resulting wave power estimates, particularly when the real sea state is comprised of multiple wave systems (for example, a local sea plus one or more swells approaching from different directions). However, since $P \propto T_e H_s^2$, errors in period are less significant than errors in wave height.

3. Methodology

3.1. Numerical models

3.1.1. Tide

The hydrodynamic model in the MIKE 21 Flow Model (MIKE 21 HD) is a general numerical modeling system for the simulation of water levels and flows in estuaries, bays and coastal areas [5]. It simulates unsteady two-dimensional flows in one layer (vertically homogeneous) fluids and has been applied in a large number of studies.

The following equations, the conservation of mass and momentum integrated over the vertical, describes the flow and water level variations:

$$\frac{\partial \zeta}{\partial t} + \frac{\partial p}{\partial x} + \frac{\partial q}{\partial y} = \frac{\partial d}{\partial t} \quad (14)$$

$$\begin{aligned} \frac{\partial p}{\partial t} + \frac{\partial}{\partial x} \left(\frac{p^2}{h} \right) + \frac{\partial}{\partial y} \left(\frac{pq}{h} \right) + gh \frac{\partial \zeta}{\partial x} + \frac{gp\sqrt{p^2+q^2}}{C^2 h^2} - \frac{1}{\rho_w} \left[\frac{\partial}{\partial x} (h\tau_{xx}) \right. \\ \left. + \frac{\partial}{\partial x} (h\tau_{xy}) \right] - \Omega q - fVv_x + \frac{h}{\rho_w} \frac{\partial}{\partial x} (p_a) \\ = 0 \end{aligned} \quad (15)$$

$$\begin{aligned} \frac{\partial p}{\partial t} + \frac{\partial}{\partial y} \left(\frac{p^2}{h} \right) + \frac{\partial}{\partial x} \left(\frac{pq}{h} \right) + gh \frac{\partial \zeta}{\partial y} + \frac{gp\sqrt{p^2+q^2}}{C^2 h^2} - \frac{1}{\rho_w} \left[\frac{\partial}{\partial y} (h\tau_{yy}) \right. \\ \left. + \frac{\partial}{\partial x} (h\tau_{xy}) \right] - \Omega q - fVv_y + \frac{h}{\rho_w} \frac{\partial}{\partial y} (p_a) \\ = 0 \end{aligned} \quad (16)$$

Where:

$h(x, y, t)$ is water depth, $C(x, y)$ is Chezy resistance, $f(V)$ stands for wind friction factor, $\Omega(x, y)$ is Coriolis Parameter-Latitude dependent-, $P_a(x, y, t)$ is atmospheric pressure, $\zeta(x, y, t)$ is surface elevation, $V, V_x, V_y(x, y, t)$ stand for wind speed and components in X- and Y-directions, $p, q(x, y, t)$ represent flux densities in X- and Y-direction ($m^3/s/m$) = (vh, uh) , (v, u) = depth-averaged velocities in X- and Y-directions, $\tau_{xx}, \tau_{xy}, \tau_{yy}$ are components of effective shear stress.

MIKE 21 HD makes use of a so-called Alternating Direction Implicit (ADI) technique to integrate the equations for mass and momentum conservation in the space–time domain. The equation

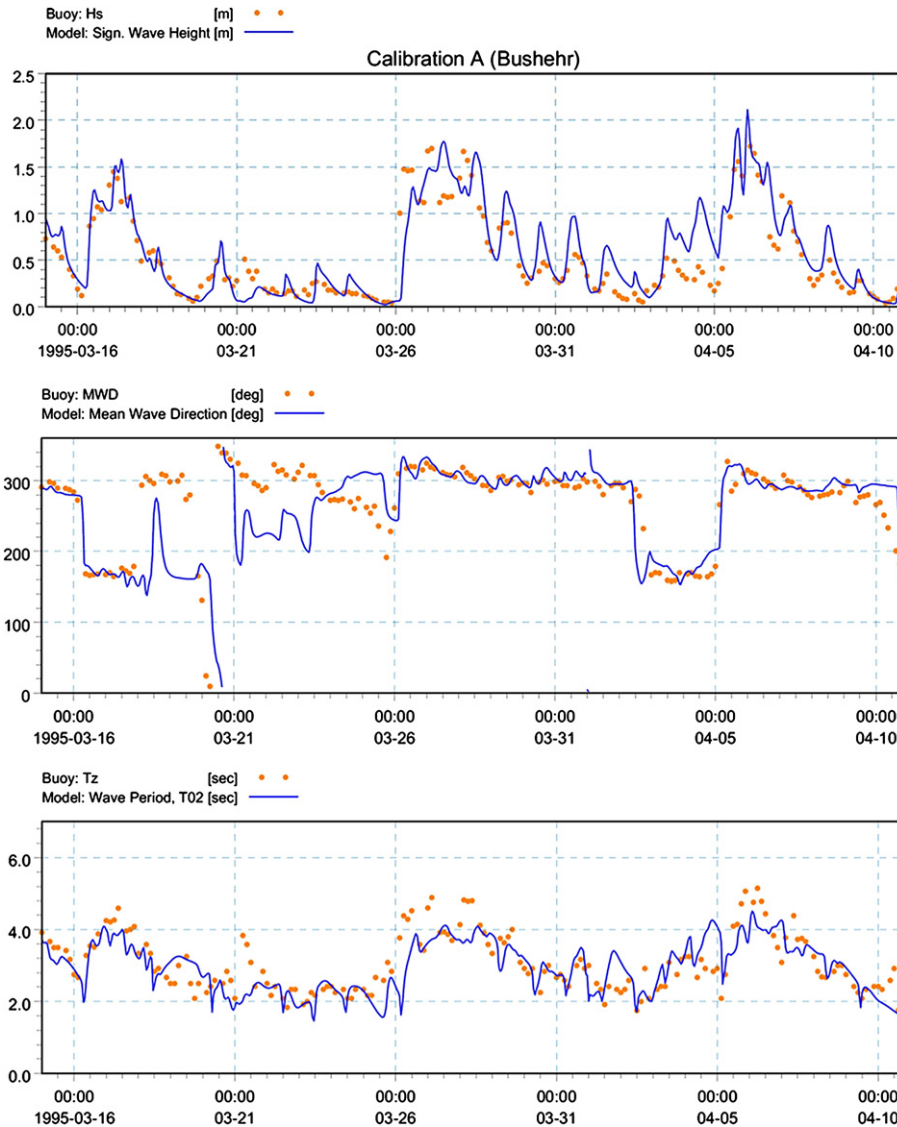


Fig. 4. Validation period (A) – Boushehr.

matrices that result for each direction and each individual grid line are resolved by Double Sweep (DS) Algorithm.

The raw bathymetry used to produce the mesh was provided by National Cartographic Center of Iran-Department of Hydrography, which had been previously digitized from the data from sounding sheets. The nominal resolution of the bathymetry in the whole area was about 50 m. The mesh was created using the Bathymetries program (part of the MIKE Zero program) and is shown in Fig. 1, overlaid on the interpolated bathymetry. The finite difference mesh is a Cartesian grid covering the Persian Gulf. Grid size is 1000 _ 1000 m within the whole area (Fig. 1). The model is run with a time step of 30 s, which according to the Courant–Friedrichs–Levy criterion is sufficiently small to ensure numerical stability. The mesh contains 653 600 nodes.

3.1.2. Wave

The estimation of the wave energy potential of Persian Gulf and Sea of Oman was carried out using a data set composed of time series of wind and wave parameters obtained by means of the ISWM (Iranian Sea Wave Model) numerical model, a third generation offshore wave model operated jointly by Iran Ports and Maritime

Organization (PMO) and Iran National Centre of Oceanography (INCO). The wind data consisting of Atmospheric model ERA40 from 1999 to 2003 is purchased from European Centre for Medium Range Weather Forecasting (ECMWF) for running the wave model, and then checked for consistency with observations and the previous evolution of the wind and pressure fields by the Iranian Meteorological Office.

The ISWM model is a new generation spectral wind-wave model based on unstructured meshed. The model simulates the growth, decay and transformation of wind-generated waves and swells in offshore and coastal areas of Persian Gulf and Sea of Oman. The wave field is described by the two-dimensional wave action density spectrum, $N(\omega, \theta)$, where ω is the angular wave frequency and θ is the wave direction. The governing equation is the wave action balanced equation formulated in either Cartesian or spherical co-ordinates. In horizontal Cartesian co-ordinates, the conservation equation for wave action can be written as

$$\frac{\partial N}{\partial t} + \nabla \cdot (\vec{v}N) = \frac{S}{\sigma} \quad (17)$$

Where $N(\vec{x}, \sigma, \theta, t)$ is the action density, t is the time, $\vec{x} = (x, y)$ is

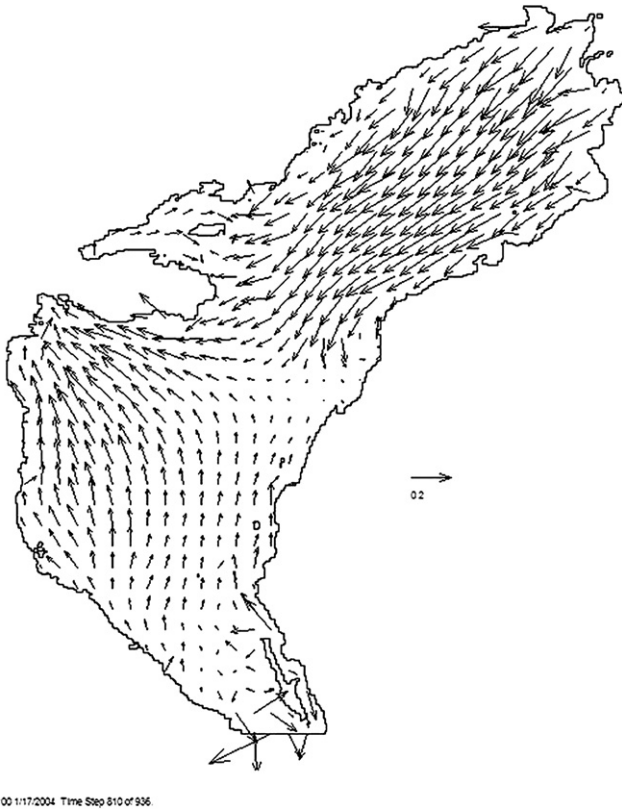


Fig. 5. mid-flood of a mean spring tide.

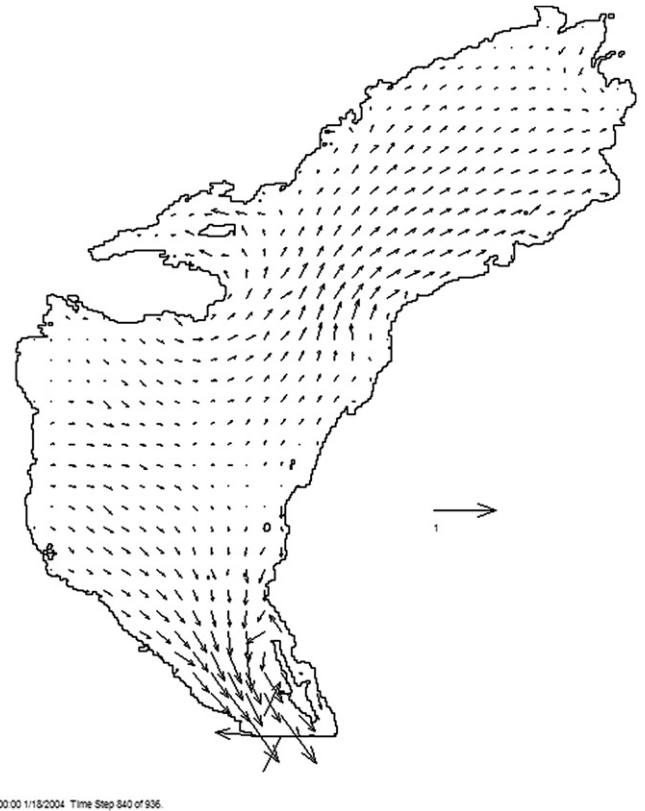


Fig. 6. mid-ebb of a mean spring tide.

the Cartesian co-ordinates, $\vec{v} = (C_x, C_y, C_\sigma, C_\theta)$ is the four-dimensional phase space \vec{x} , σ and θ , and S is the source term for the energy balance equation. ∇ is the four-dimensional differential operator in the \vec{x} , σ , θ -space. The four characteristic propagation speeds are given by

$$\begin{aligned} (c_x, c_y) &= \frac{d\vec{x}}{dt} = \vec{c}_g + \vec{U} \\ c_\sigma &= \frac{d\sigma}{dt} = \frac{\partial \sigma}{\partial d} \left[\frac{\partial d}{\partial t} + \vec{U} \cdot \nabla_{\vec{x}} d \right] - c_g \vec{k} \cdot \frac{\partial \vec{U}}{\partial s} \\ c_\theta &= \frac{d\theta}{dt} = -\frac{1}{k} \left[\frac{\partial \sigma}{\partial d} \frac{\partial d}{\partial m} + \vec{k} \cdot \frac{\partial \vec{U}}{\partial m} \right] \end{aligned} \quad (18)$$

Here, s is the space co-ordination in wave direction θ , and m is a co-ordinate perpendicular to s . $\nabla_{\vec{x}}$ is the two-dimensional differential operator in the \vec{x} -space. [6]

Based on the directional wave energy spectra it is possible to compute the wave parameters of interest. The expressions of some of these parameters are presented below for convenience [7]. Denoting the directional wave energy spectrum by $S(f, \theta)$, with f the wave frequency, the spectral moments are defined as

$$\int_0^{2\pi} \int_0^\infty f^n S(f, \theta) df d\theta \quad n = 0, 1, 2, \dots \quad (19)$$

The significant wave height is given by

$$H_s = 4m_0^{1/2} \quad (20)$$

and the peak wave period is the inverse of the frequency at the spectral peak (f_p),

$$T_p = (f_p)^{-1} \quad (21)$$

The wave power, also known as the wave energy flux, is given by equation (5). Seawater density depends on salinity and temperature, which vary in time and space; an average value was taken for this work $\rho = 1025 \text{ kg/m}^3$. Equation (8) yields the wave power per unit width of wave front; if a certain wave energy converter (WEC) captures the energy of a width b of wave front, the corresponding power is $P_{WEC} = Pb$.

Naturally the actual power output will depend on the converter efficiency. The mean wave direction may be obtained from the directional wave energy spectrum through

$$\theta_m = \arctan \frac{\int_0^{2\pi} \int_0^\infty S(f, \theta) \sin \theta df d\theta}{\int_0^{2\pi} \int_0^\infty S(f, \theta) \cos \theta df d\theta} \quad (22)$$

3.2. Numerical model validation

3.2.1. Tidal model validation

The forcing factors taken into account by the model are the tide, the wind, and the discharge into Persian Gulf of the Arvand River. At the ocean boundary, the tidal elevation is computed at each time step by using the in-situ measurement data from National Cartographic Center of Iran – Department of Hydrography’s website. The wind velocity and direction data for the time period from January 1992–2003 is purchased from European Centre for Medium Range Weather Forecasting (ECMWF) by the Port and Maritime Organization. These data were input to the model at 6-Hour intervals during the validation period, assuming a varying in time and space wind

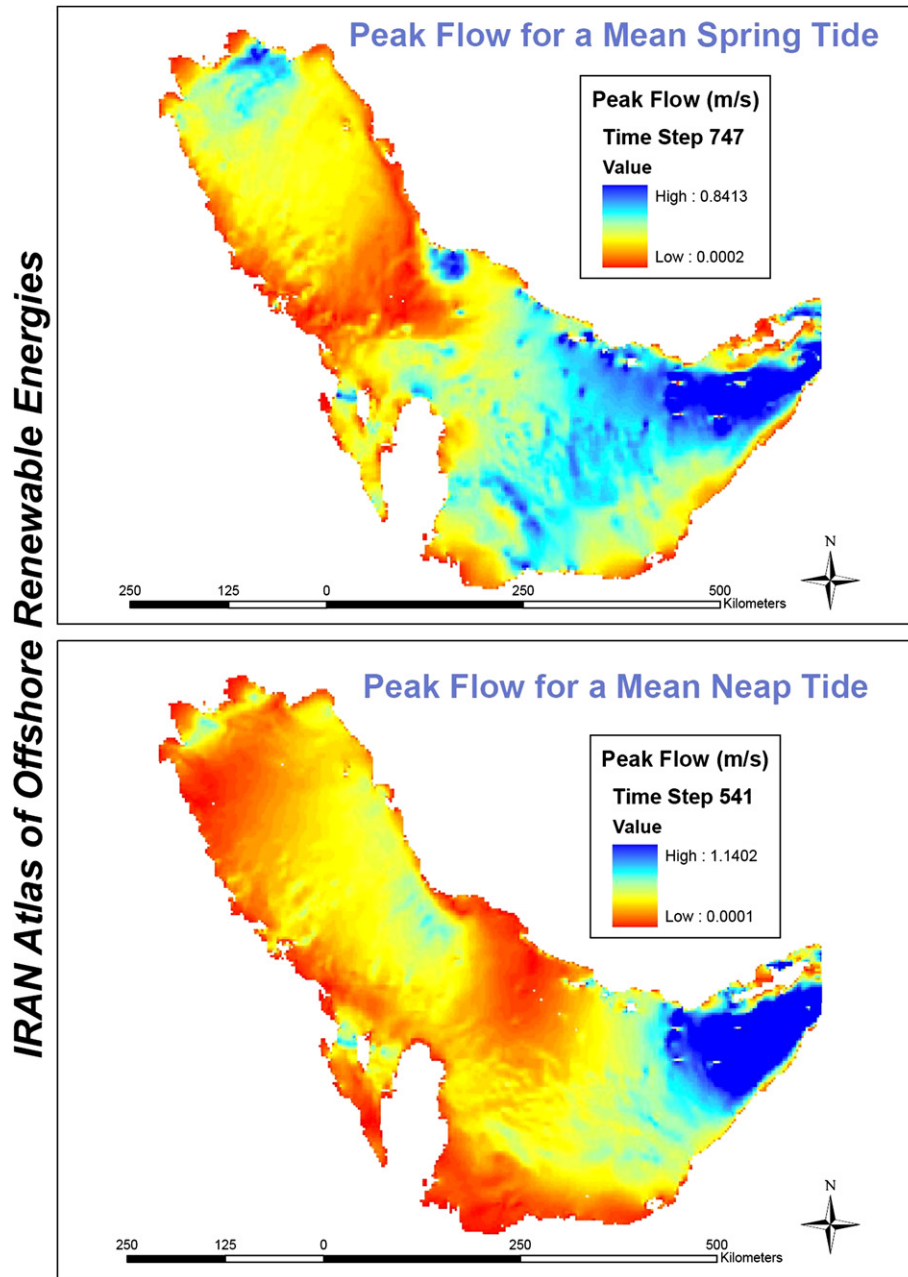


Fig. 7. Peak flow for a Mean Spring Tide (upper map) and a Mean Neap Tide (lower map).

type over the Persian Gulf. River discharge data were input to the model based on statistical data available.

An example of validation for a tidal model is to compare the predicted height of the tide with that observed at several locations [1]. Accurate records of tidal elevations are made at standard ports around IRAN. Predicted tidal elevation amplitude from a model can be compared with measured amplitudes wherever data is available. One way of visualizing the comparison is to plot model vs. actual tide height on a simple scatter diagram.

Four tidal components, representing the more important tidal components, have been selected for assessment here; these are the diurnal constituents O1 and K1, semi-diurnal constituents M2 and S2. These are compared against data interpolated from admiralty charts.

Fig. 2 shows the comparison between the phases of Admiralty Data and model datasets for those four components. The scatter plots

show model and extracted values together with a line of perfect agreement and show that the model is generally in good agreement with the interpolated tidal constituents. This is further supported by the mean and root mean square (RMS) differences (shown above each plot and provided in Table 1). These small differences mostly come from inaccuracy in the process of interpolation of the Admiralty's charts, since there were no accurate observed values covering whole area of Persian Gulf so the void points were interpolated through a logical process at the GIS environment.

3.2.2. Wave model validation

The validation exercise was undertaken in 4 parts. To test validity against a measured source and geographic variation in performance, ISWM results and observation time series from in-situ wave and meteorological measurement platforms were compared. Table 3 summarizes the stations and the validation period for which the

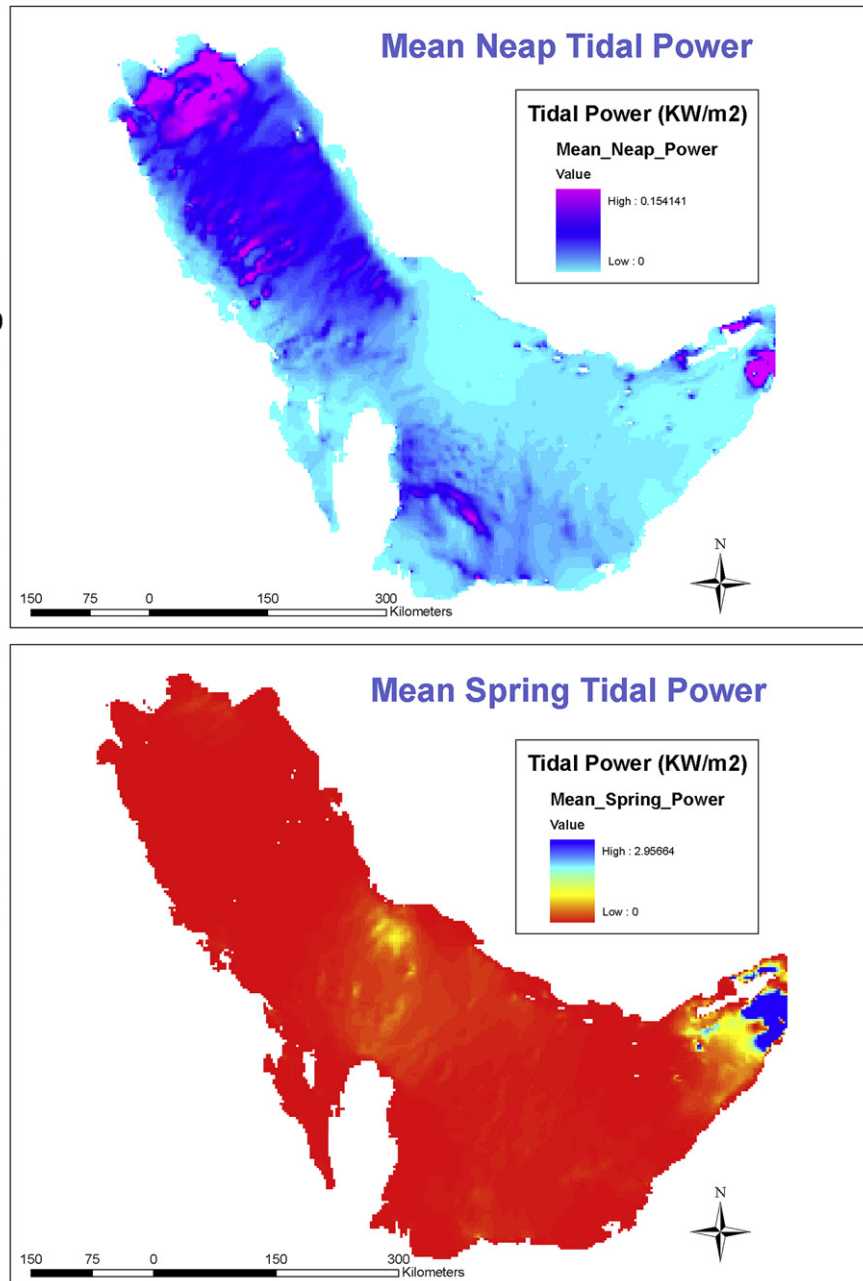


Fig. 8. Mean Neap Tidal Power (upper map) and Mean Spring Tidal Power (lower map).

comparison has made. These sites provide observations of wave parameters listed in Table 3.

Model was run several times with different values for wave breaking, bottom friction, and white capping coefficient. The results from each run were compared with the in-situ measurements and show a good agreement between model results and buoys data [8]. The final values for the coefficients are presented in Table 2.

Fig. 4 shows the simulation results for Calibration period (A) compared with the buoy data in that period.

4. Results and discussions

4.1. Tide

Having been validated, the model can now be used to calculate the tidal flow velocities over the Persian Gulf. For this purpose it is

run without including the wind among the forcing factors, as the aim of this work is to quantify the tidal stream resource. Figs. 5 and 6 show the flow velocity vectors at mid-flood and mid-ebb of a mean spring tide respectively. It is apparent that the highest velocities occur in the area near the HORMOZ Strait, due to the constriction imposed on the flow by the approaching margins. In almost whole area except for limited number areas, current velocities are lower than 1 m/s, the minimum value for economic operation of a tidal stream power plant [9].

The largest current magnitudes in the Persian Gulf, on the order of 1.5 m/s, are found along the cross-section between LOFT Jetty (GHESHM Island) and Pt. POHL, where the strait width decreases to a mere 2400 m. Now the power density can be computed applying Equation (1).

The power density in the Persian Gulf is represented in Fig. 8 at a mean spring tide and a mean neap tide. On the flooding tide, the

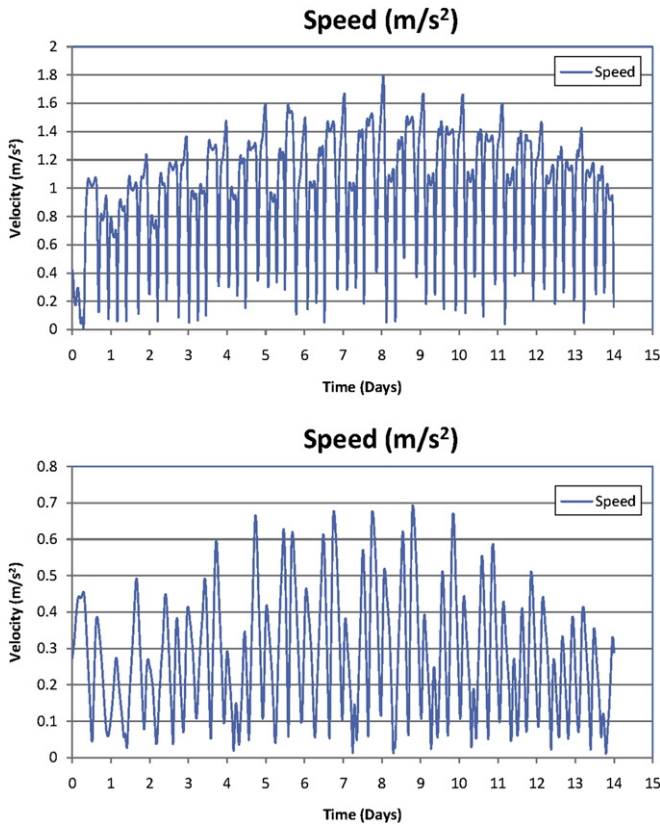


Fig. 9. Flow velocity at points A (upper graph) and B (lower graph) throughout a 14-day spring–neap cycle.

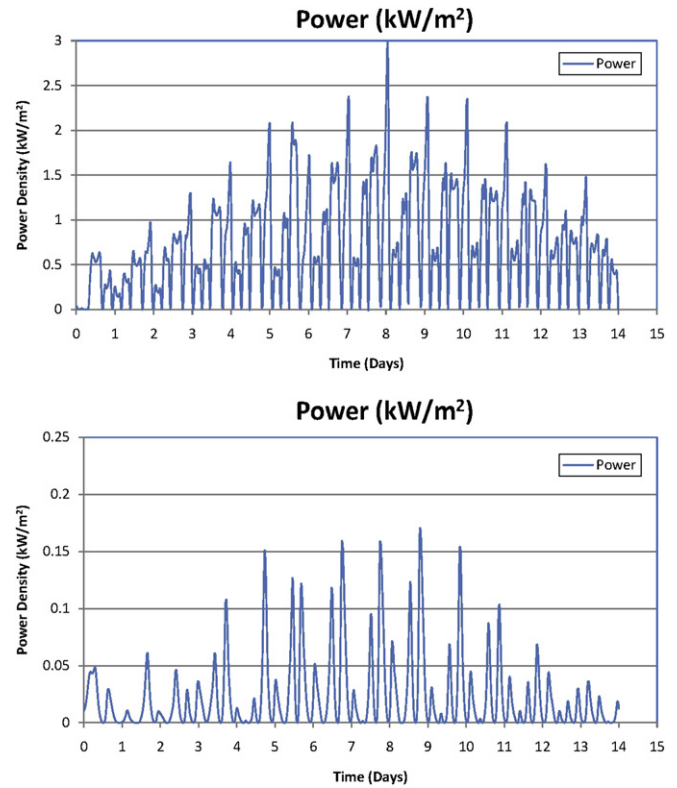


Fig. 10. Power density at points A (upper graph) and B (lower graph) throughout a 14-day spring–neap cycle.

highest power densities, above 2.5 kW/m², are found in a small area close to Pt. POHL; during the ebb, the power density is considerably smaller as the somewhat lower current velocities are cubed in Equation (1).

In order to characterize with more precision the tidal stream resource, two locations are chosen: point A (Pt. POHL) in the zone with the highest power density, and point B (Abu Musa Island) in an area with a lower power density. The velocity magnitude at both points is shown in Fig. 9 during a 14-day period, so as to cover the spring–neap variation. Peak values in spring are 1.8 and 0.7 m/s at points A and B, respectively.

Fig. 10 shows the time distribution of the power density at both points. The difference in peak velocity between them is

amplified by the cubic exponent, resulting in a large disparity in power density values: 3 kW/m² and 0.17 kW/m² at points A and B, respectively. For the 14-day period considered, the energy density, or energy per square meter of turbine aperture, available at each point is the area under the curve in Fig. 7. A numerical integration yields 244.44 and 7.84 kWh/m² for points A and B, respectively. The annual figures are 6373.126 and 204.409 kWh/m² respectively. Assuming a power coefficient $C_p = 0.33$ in accordance with [10], the annual energy output is 2103.131 and 67.454 kWh per square meter of turbine aperture at points A and B, respectively. With a turbine aperture of 750 m², in the range of other tidal stream plants recently proposed [11] the annual energy output would be 1577.3488 MWh and 50.591 MWh at points A and B, respectively.

Table 4
% of total time in an average year corresponding to sea states with different significant wave height (HS) and peak wave period (TP) point 1-29.

H _S (m)	Percentage of Occurrence											Total	
	T _P (s)	≤2	2–4	4–6	6–8	8–10	10–12	12–14	14–16	16–18	18–20		>20
>8	0.00	0.00	0.00	0.00	0.00	0.00	0.00	0.00	0.00	0.00	0.00	0.00	0.00
7–8	0.00	0.00	0.00	0.00	0.00	0.00	0.00	0.00	0.00	0.00	0.00	0.00	0.00
6–7	0.00	0.00	0.00	0.00	0.00	0.00	0.00	0.00	0.00	0.00	0.00	0.00	0.00
5–6	0.00	0.00	0.00	0.00	0.00	0.00	0.00	0.00	0.00	0.00	0.00	0.00	0.00
4–5	0.00	0.00	0.00	0.00	0.00	0.00	0.00	0.00	0.00	0.00	0.00	0.00	0.00
3–4	0.00	0.00	0.00	0.01	0.00	0.00	0.00	0.00	0.00	0.00	0.00	0.00	0.01
2–3	0.00	0.00	0.01	0.11	0.00	0.00	0.01	0.00	0.00	0.00	0.00	0.00	0.14
1–2	0.00	0.01	2.15	0.11	0.03	0.04	0.30	0.04	0.00	0.00	0.00	0.00	2.68
0.5–1	0.00	15.92	13.36	2.31	3.83	5.41	0.73	0.14	0.05	0.05	0.00	0.00	41.81
<0.5	0.00	5.69	8.58	2.63	27.84	9.39	1.00	0.14	0.00	0.08	0.00	0.00	55.36
Total	0.00	21.63	24.11	5.17	31.70	14.84	2.04	0.31	0.05	0.14	0.00	0.00	100.00

Table 5
% of total time in an average year corresponding to sea states with different range of mean wave direction (θ_m) and significant wave height (HS) point 1-29.

Percentage of Occurrence											
Direction	H_s (m)										Total
	<0.5	0.5–1	1–2	2–3	3–4	4–5	5–6	6–7	7–8	>8	
N	0.81	0.51	0.00	0.00	0.00	0.00	0.00	0.00	0.00	0.00	1.31
NE	0.59	0.40	0.00	0.00	0.00	0.00	0.00	0.00	0.00	0.00	0.99
E	1.96	2.37	0.29	0.00	0.00	0.00	0.00	0.00	0.00	0.00	4.61
SE	43.03	17.95	0.88	0.01	0.00	0.00	0.00	0.00	0.00	0.00	61.86
S	1.56	0.59	0.03	0.00	0.00	0.00	0.00	0.00	0.00	0.00	2.18
SW	0.79	0.97	0.00	0.00	0.00	0.00	0.00	0.00	0.00	0.00	1.77
W	2.05	6.57	1.18	0.12	0.01	0.00	0.00	0.00	0.00	0.00	9.94
NW	4.57	12.46	0.31	0.00	0.00	0.00	0.00	0.00	0.00	0.00	17.34
Total	55.36	41.81	2.68	0.14	0.01	0.00	0.00	0.00	0.00	0.00	100.00

4.2. Wave

The ISWM model grid nodes nearest to the IRAN shoreline– 19 points (Fig. 3) were selected to characterize the wave energy potential. The six-hourly values of significant wave height, peak period, and mean wave direction within the period 1997–2003 were analyzed for each point. To this end, the joint (H_s, T_p) distribution was discretised considering eleven significant wave height intervals and similarly eleven peak period intervals, leading to 110 combined intervals. Ascribing each six-hourly sea state to the appropriate interval, the percentage of the total time in an average year corresponding to the different intervals was obtained. For illustration Table 4 shows the results for grid point 1-29.

A similar analysis was carried out combining mean wave direction and significant wave height. Eight sectors were considered for the mean wave direction (N, NE, E, SE, S, SW, W and NW). With the same significant wave height intervals as before, 88 combined intervals of the (H_s, θ_m) distribution ensued. The sea states in the period 1997–2003 were ascribed to these intervals and the corresponding time percentages computed (Table 5 for grid point 1-29).

For the computation and characterization of wave energy at each point, the wave spectra were assumed to hold during the lapse between consecutive data, i.e. 6 h. The wave energy in the sea states of each of the combined (H_s, T_p) and (H_s, θ_m) intervals in the 1997–2003 period was calculated and referred to a one-year period to obtain the value in an average year; the total annual wave energy was obtained as the sum of all the intervals. This procedure was repeated for each point; Table 6 shows the results of the (H_s, T_p) analysis at point 1-29, with wave energy data expressed in KWh per unit width of wave front [12].

5. Conclusion

The study has provided a preliminary assessment of the different levels of the mean annual wave and tidal power/energy resource that are available around Iran. It amplifies earlier studies and quantifies the electrical resource in a way that allows recognition of particularly promising areas and comparison with other Renewables.

A 2D finite element numerical model has been constructed to simulate tidal flows across the Persian Gulf. The ability of the model to reproduce features of the tidal stream has been shown to be reasonable and the results of the model have been used in an example to predict the power output from a turbine located off the coast of Iran.

In comparison to tides, the wave resource is more difficult to predict due to the 'random' behavior of the meteorological driving conditions. It is standard practice to describe the wave regime by consideration of a long-term measure of the wave record, commonly over several years so that year-to-year variations are averaged out. The wind and wave datasets have been derived from an archive called "ISWM" (5 years, 1998–2003) which has been modeled by MIKE 21 SW, and validated against the in-situ measurements. The wave resource assessment includes statistics that differentiate between the energy that can be exploited by focusing a device on the primary component of energy in the wave field, as compared to the energy available to devices that can capture the total energy from sea states comprising distinct wind-wave and swell components.

In order to reduce the results of the modeling to a usable form, a spatial database of tidal stream harmonic constituents at points on a grid was created through the GIS techniques. This is integrated into a database of wider information such as bathymetry and potential constraints for development. "The Atlas" may be further developed

Table 6
Annual wave energy corresponding to sea states in different ranges of significant wave height (HS) and peak wave period (TP). Point 1-29.

> H_s (m)	T_p (s)												Total	
		≤ 2	2–4	4–6	6–8	8–10	10–12	12–14	14–16	16–18	18–20	>20		
>8	E (KWh/m)	0.00	0.00	0.00	0.00	0.00	0.00	0.00	0.00	0.00	0.00	0.00	0.00	0.00
7–8		0.00	0.00	0.00	0.00	0.00	0.00	0.00	0.00	0.00	0.00	0.00	0.00	0.00
6–7		0.00	0.00	0.00	0.00	0.00	0.00	0.00	0.00	0.00	0.00	0.00	0.00	0.00
5–6		0.00	0.00	0.00	0.00	0.00	0.00	0.00	0.00	0.00	0.00	0.00	0.00	0.00
4–5		0.00	0.00	0.00	0.00	0.00	0.00	0.00	0.00	0.00	0.00	0.00	0.00	0.00
3–4		0.00	0.00	0.00	6.48	0.00	0.00	0.00	0.00	0.00	0.00	0.00	0.00	6.48
2–3		0.00	0.00	2.48	25.7	0.00	0.00	5.08	0.00	0.00	0.00	0.00	0.00	33.28
1–2		0.00	0.35	107.3	11.7	2.58	6.92	59.67	8.00	0.00	0.00	0.00	0.00	196.58
0.5–1		0.00	149.8	202.5	35.9	81.59	140.6	22.92	5.44	1.78	1.76	0.00	0.00	642.49
<0.5		0.00	20.94	48.18	17.3	199.9	102.1	12.57	1.71	0.00	2.11	0.00	0.00	404.86
Total		0.00	171.16	360.59	97.14	284.07	249.70	100.2	15.14	1.78	3.88	0.00	0.00	1283.69

to incorporate additional data layers, which often already exist, providing information on existing infrastructures (cables, pipelines, oil and gas installations, aquaculture), activities (navigation, leisure, fishing), and environmental considerations (designations, flora, and fauna). The final database, in conjunction with a separate set of turbine parameters including a speed–efficiency curve, would enhance understanding of potentially exploitable resource areas to deploy rated devices. Further work can also concentrate on including in the model the effects of placing a number of tidal stream power generating units in the flow.

References

- [1] Hardisty J. Estuaries: monitoring and modeling the physical system. Oxford: Blackwells; 2007.
- [2] Atlas of UK marine renewable energy resources: technical report. ABP Marine Environmental Research Ltd.; 2004. Report No. R.1106 prepared for the UK Department of Trade and Industry.
- [3] Hagerman, G. Southern New England Wave Energy Resource Potential. In: Proc. Building Energy 2001, Boston, USA; 2001.
- [4] Cornett AM. A global wave energy resource assessment, International Offshore and Polar Engineering Conference 2008. Canada: Vancouver; 2008.
- [5] MIKE 21 Manual, MIKE21 HD scientific documentation; 2005.
- [6] MIKE 21 Manual, MIKE21 SW scientific documentation; 2005.
- [7] Holthuijsen LH. Waves in oceanic and coastal waters. Cambridge University Press; 2007.
- [8] Technical report, ISWM Iranian sea wave modeling. Phase 3, ports and maritime organization. See URL: <http://coastseng.pmo.ir/coastalengineeringoffice-proj17-proj19-fa.html>; 2008.
- [9] Bahaj AS, Myers L. Analytical estimates of the energy yield potential from the Alderney Race (Channel Islands) using marine current energy converters. Renewable Energy 2004;29:1931–45.
- [10] Carballo R, Iglesias G, Castro A. Numerical model evaluation of tidal stream energy resources in the Ria de Muros (NW Spain). Renewable Energy 2009;34:1517–24.
- [11] Brooks DA. The tidal-stream energy resource in Passamaquoddy – Cobscook Bays: a fresh look at an old story. Renewable Energy 2006;31:2284–95.
- [12] Iglesias G, Lopez M, Carballo R, Castro A, Fraguera JA, Frigaard P. Wave energy potential in Galicia (NW Spain). Renewable Energy 2009; 34:1333–2323.